Pesquisa Operacional (2022) 42(nspe1): e264770 p.1-30
doi: 10.1590/0101-7438.2022.042nspe1.00264770

Printed version ISSN 0101-7438 / Online version ISSN 1678-5142
www.scielo.br/pope
ARTICLES

A DIAGNOSTICS AND PROGNOSTICS FRAMEWORK FOR MULTI-COMPONENT SYSTEMS WITH WEAR INTERACTIONS: APPLICATION TO A GEARBOX-PLATFORM

Roy Assaf[1], Phuc Do[2*] and Phil Scarf[3]

Received June 7, 2022 / Accepted June 28, 2022

ABSTRACT. We present a novel framework for diagnostics and prognostics for multi-component systems with wear interaction between components. The principal elements of this framework are: health-state indicator extraction using signal-processing; clustering of wear phases using a Gaussian mixture model; a stochastic multivariate wear model; and prediction of the remaining-useful-life of components using particle-filtering. These elements of the framework are illustrated and verified using an experimental platform that generates real data. Our diagnostics study shows that different clusters not only indicate the wear-state, but also the wear-rate of the components. Furthermore, our prognostics study shows that the wear-interaction between components has an significant impact in predicting the remaining-useful-life for components. Thus, we demonstrate, for prognostics and health management, the importance of modeling wear interactions in the prognostic process of multi-component systems.

Keywords: prognostics and health management, multi-component system, reliability, maintenance, remaining-useful-life, wear interaction.

1 INTRODUCTION

Systems with interactions that relate to the transfer of energy, heat and work, will eventually degrade. This is the case of most machinery, whether mechanical or electronic. Such degradation or wear may lead to failure, unexpected downtime and hence lower equipment-effectiveness and higher costs. Nonetheless, wear processes may be slowed or even prevented by maintenance intervention. The literature on maintenance suggests that the recent major advances in the field have been in condition-based maintenance (CBM) and in prognostics and health management

*Corresponding author
[1]School of Computing, Science & Engineering, Autonomous Systems and Robotics Centre, University of Salford, Manchester, M5 4WT, UK – E-mail: royassaf1.618@gmail.com
[2]Université de Lorraine, CRAN, UMR 7039, Campus Sciences, BP 70239, Vandoeuvre-les-Nancy, 54506, France – E-mail: phuc.do@univ-lorraine.fr – http://orcid.org/0000-0003-4113-5895
[3]Cardiff Business School, Cardiff University, Cardiff, CF10 3AT, UK – E-mail: ScarfP@cardiff.ac.uk – http://orcid.org/0000-0001-5623-906X

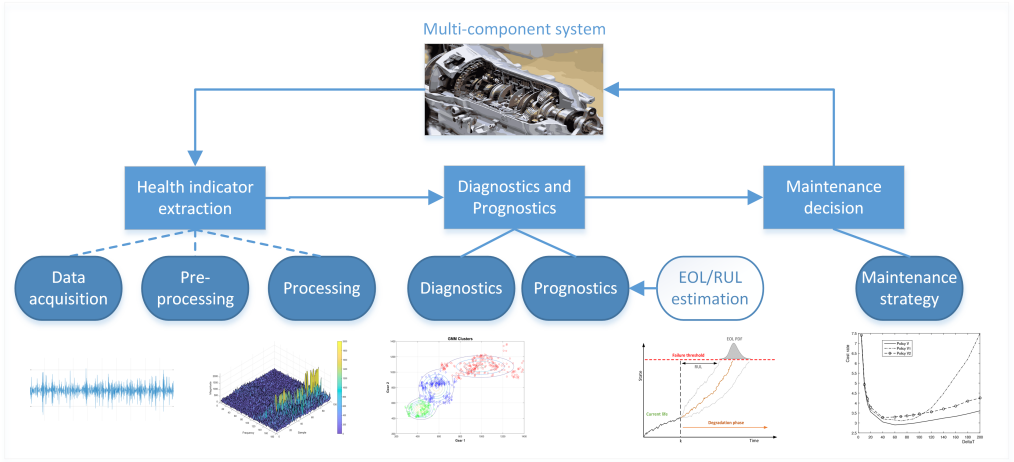

Figure 1 – Principal elements of prognostics and health management.

(PHM) Zio (2021). CBM, in contrast to traditional maintenance policies, is proactive in nature, aiming to maintain systems only when needed Grall et al. (2002); Jardine et al. (2006); Peng et al. (2010). PHM has many similarities with CBM Kim et al. (2017); Wang et al. (2017), and is principally seen as a key enabler for it Vachtsevanos et al. (2006). Notionally, the focus of CBM is the optimization of maintenance policy for a system, and the focus of PHM is the assessment (diagnosis) and prediction (prognosis) of the health-state of a system, with assessments made in real time in both approaches Jimenez et al. (2020). Thus, compared to CBM, PHM deals largely with extraction of the indicators of health-state from measured signals and puts greater emphasis on diagnosis and prognosis, which is essential for the optimization of maintenance decisions. In this paper, we also emphasize diagnosis and prognosis.

Freitas et al. (2010) Reliability assessment using degradation models: Bayesian and classical approaches

For a maintained system, the first step in the PHM approach is health-state indicator extraction. Next, these health-indicators are used for diagnosis and prognosis. Then follows maintenance optimization using outputs from diagnostic and prognostic analysis. In the optimization step, the objective is to reduce maintenance cost and/or to increase the system reliability or availability. These steps are illustrated in Figure 1.

In analyses of this type, it is typically assumed that the wear processes of individual components are independent Bouvard et al. (2011); Nguyen et al. (2014); Nguyen & Medjaher (2019); Van Noortwijk (2009), thereby reducing the effectiveness of derived PHM and CBM policies because real-world systems typically possess many interacting components. Indeed, in Frei et al. (2013), the authors suggest that it is often more plausible that failures are dependent than independent. Furthermore, while interest in the CBM literature in dependencies in multi-component systems is growing, the modeling of stochastic dependence is the least ex-

plored Keizer et al. (2017); Nicolai et al. (2009). Also, stochastic dependence of components, as opposed to economic dependence of components (e.g. shared set-up costs), arguably falls more within PHM than CBM, because wear-interactions impact directly upon component lifetimes and indirectly upon costs. Therefore, it is important to consider stochastic dependence in PHM of multi-component systems. However, to the best of our knowledge, no existing PHM framework allows taking into account this kind of dependence between components. To face this challenge, we propose a novel PHM framework allowing to consider the wear interactions between components.

The framework itself is a collection of methods for diagnosis and prognosis:

- A method based on short-time Fourier transform for the effective extraction of health-state indicators for each component in a multi-component system;
- A diagnostics method using Gaussian mixture model (GMM) to detect different wear phases given stochastic dependence between components;
- A prognostic method based on a multi-component degradation model coupled with particle filtering to predict the remaining-useful-life of each component with consideration of wear-interaction impacts.

The proposed framework is then applied to the data collected on a gearbox experimental platform.

The structure of the paper departs somewhat from this ordering of the elements of the framework. This is because we first present theory in Section 2 relating to dependencies in multi-component systems, Gaussian mixture models, particle filtering, and multivariate wear models. Then, the methodology for health-indicator extraction of multi-component systems is considered in Section 3. Section 4 describes the experimental platform, the generation of data on the platform, and health-indicator extraction for its critical components. Section 5 describes the application of Gaussian mixture models for diagnosis. Section 6 describes the application of particle filtering for prognosis, wherein we are particularly interested to compare end-of-life predictions when we take account of stochastic dependence (through modeling) and when we do not. Finally, in Section 7 we conclude with a review of our approach and its findings, limitations and opportunities for further development.

2 DIAGNOSTICS AND PROGNOSTICS FOR A MULTI-COMPONENT SYSTEM WITH WEAR INTERACTIONS

2.1 Background and classification of stochastic dependence

The current literature on CBM and PHM focuses principally on one-component systems. This is in part because the analysis of stochastic models and the characteristics of optimal CBM policies are much more complicated for multi-component systems Alaswad & Xiang (2017).

In the literature reviews that mainly deal with the maintenance of multi-component systems De Jonge & Scarf (2020); Dekker et al. (1997); Dinh et al. (2020); Nicolai & Dekker (2008);

Thomas (1986), component dependencies are generally classified as: structural dependence; economic dependence; and stochastic dependence. A fourth type of dependence, resource dependence, is also discussed in Keizer et al. (2017). Multi-component dependencies are fundamental to our paper. In particular, we will consider stochastic dependence in detail throughout this work. A general representation of multi-component dependencies is shown in Figure 2.

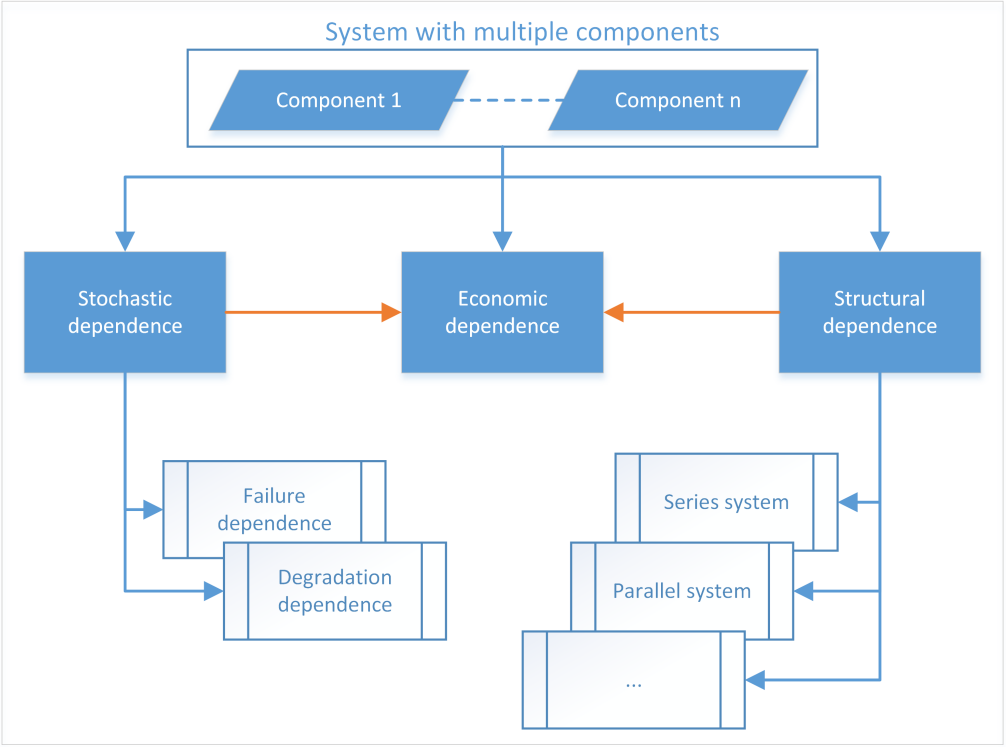

Figure 2 – An overview of multi-component dependencies.

Stochastic dependence is principally concerned with the question of how the health-state of one component influences the health-state of other components in a multi-component system. Health-state itself can be characterized in many ways: as a binary variable (failed, not failed); as age of the component; as performance; as a measure determined from condition monitoring; or as a combination of some or all of these.

We differentiate stochastic dependencies into two groups: failure interaction; and wear interaction. In failure interaction, failure of one component impacts upon the state of other components. There are then implications for maintenance policy, see for example Scarf & Deara (1998), where age-based replacement and opportunistic age-based maintenance policies are studied when there is type I failure interaction, and Satow & Osaki (2003), where damage accumulates in component 2 as a result of failures of component 1. In contrast, in wear interaction, the health-state of one functioning component influences the wear-rates of other functioning components. Recent works

Assaf et al. (2016); Bian & Gebraeel (2014); Rasmekomen & Parlikad (2016) call this rate-state interaction, and it can include common-mode deterioration. Reasons for the recent growing interest in rate-state interactions is development of sensor technology and IoT (internet of things) that facilitate more extensive condition monitoring and the development of approaches for prognosis and PHM in general.

This paper focuses on wear interaction and we describe our model in detail in Section 2.3. However, we first we discuss our diagnostic and prognostic approaches for handling such interaction.

2.2 Diagnostics using a Gaussian mixture model

The previous discussion suggests that stochastic dependence may accelerate the wear-rate of components leading to unexpected faults and failures that may reduce system performance. Thus although many works exist that involve data driven diagnostics Hao et al. (2014); Hoseinzadeh et al. (2018), it remains important to address the wear-rate acceleration within the diagnosis model.

Our framework for diagnostics using a Gaussian mixture model (Figure 3) first clusters the extracted health-state data. This requires the specification of a number of clusters that should be extracted from the data. Then, it aims to diagnose the system by assigning different wear-states and rates to each data cluster. Thus, the aim of the proposed diagnostics approach is to accurately diagnose different wear-states and wear-rates of interacting components.

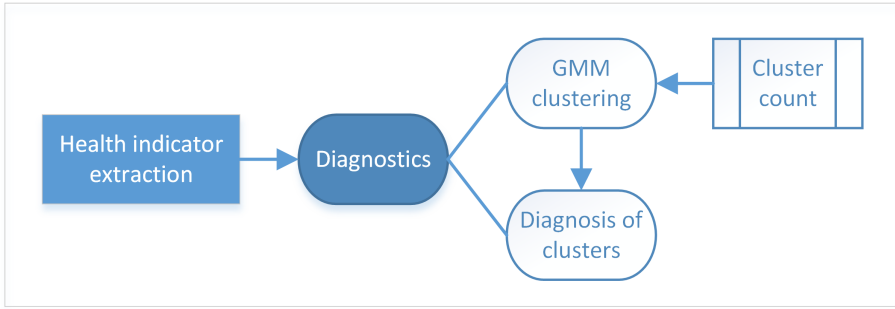

Figure 3 – A framework for diagnostics using a Gaussian mixture model.

In the paper we use GMMs for clustering. An advantage of GMMs is that a statistical criterion can be used to optimize the number of clusters Dasgupta & Raftery (1998); Ouyang et al. (2004), whereas many classical clustering algorithms such as hierarchical clustering, self-organizing maps, k-means and fuzzy C-means are largely heuristic and so do not rigorously choose the optimal number of clusters Yeung et al. (2001). Successful applications of GMM-based clustering have been reported in the literature Celeux & Govaert (1995); Yajima et al. (2015).

To train the GMM, we start with several mixture components, indexed by c, each described by a Gaussian distribution with mean μ_c and covariance σ_c, and a mixing coefficient π_c. The joint probability distribution of the GMM is then the weighted average of the C individual components:

$$p(x) = \sum_{c=1}^{C} \pi_c \mathcal{N}(x; \mu_c, \sigma_c). \tag{1}$$

In the EM algorithm, the E step assigns data points to clusters and the M step is the estimation of μ_c and σ_c for each cluster. The EM algorithm is a form of coordinate descent, so it is guaranteed to converge Wu et al. (1983). In practice, the algorithm terminates once the change in the parameters or the log likelihood at each step is sufficiently small. However, convergence to a global optimum is not guaranteed. This is best accommodated using multiple initialization. A new, unseen data point is assigned to a specific cluster using the E step.

Determining C, the number of clusters uses a separate procedure, and this is a major issue in the general case of unsupervised learning. We use the silhouette method, as recommended by Rousseeuw (1987). The method iterates between different cluster numbers, and computes a silhouette coefficient, between $+1$ and -1, for each data point. A coefficient close to $+1$ indicates that the data point is far from the neighboring clusters, and a coefficient close to -1 indicates that the data point is in the wrong cluster. Therefore, the aim is to iterate between different cluster counts and use the one that achieves the largest average silhouette coefficient across all clusters.

Note, because we aim to classify different wear phases, it is important to use more than two clusters. This is because it is desirable to allow degradation behavior to transition from nominal to critical via an intermediate, defective phase, during which fault or failure prevention measures can be taken.

2.3 Prognosis using a multivariate wear model coupled with particle filtering

Data driven prognostics makes use of data collected from sensors to predict the evolution of a representative health-state for the monitored component. The main goal of the predictions is to estimate the (time of) end-of-life, and accordingly the remaining-useful-life (RUL) of this component Saxena et al. (2008). Many works exist on this aspect Freitas et al. (2010); Wang et al. (2019); Wu et al. (2019); Yan et al. (2019). However these approaches do not consider the stochastic interaction between components and can therefore miss valuable information about the degradation rates of components.

We now describe our approach for performing prognosis for multi-component systems. We start with the multivariate wear model Assaf et al. (2018), and then show how this is coupled with particle filter PF to enable effective prognostics of multi-component systems.

Consider a multi-component system with n_c components. Suppose the wear-state of component i is described by a scalar random variable X_t^i and component i fails when X_t^i first crosses a threshold L^i. Suppose also that the system fails if any component fails and that if a component

is not operating, for whatever reason, its wear-state remains unchanged unless a maintenance intervention is carried out. Let

$$X_{t+1}^i = X_t^i + \Delta X_t^i. \tag{2}$$

We call ΔX_t^i the wear increment of component i during one time step.

Suppose that the wear of a component i at time step t may depend on the operating conditions, the state of component i, and also the state of other components, to a varying degree. Thus, in a general stationary model for the increment ΔX_t^i, we propose that:

$$\Delta X_t^i = \Delta O_t^i + \Delta X_t^{ii} + \sum_{j \neq i} \Delta X_t^{ji}. \tag{3}$$

Here ΔO_t^i is the wear increment of component i caused by the operating conditions during one time step t. ΔO_t^i can be specified deterministically or stochastically. ΔX_t^{ii} is the wear increment that is intrinsic to i at time step t. That is, ΔX_t^{ii} depends on the wear-state of component i at time step t. ΔX_t^{ii} can also be specified deterministically or stochastically. $\sum_{j \neq i} \Delta X_t^{ji}$ is the sum of all wear increments that are caused by the interaction of component i with the other components of the system. Again, this may be deterministic or stochastic.

In this paper we suppose $\Delta X^{ii} > 0$ and $\Delta X^{ji} > 0$, so that components are stochastically dependent and a wear increment of component i may depend on both the state of component i and the state of other components.

We use the following model to quantify the wear interaction between the components:

$$\Delta X_t^{ji} = \mu^{ji} \times (X_t^j)^{\sigma^{ji}} \tag{4}$$

where X_t^{ji} is the wear impact of component j on component i at time t. μ^{ji} and σ^{ji} are non-negative real numbers that quantify the effect of component j on component i, see Table 1.

Table 1 – Wear interactions between multiple components.

Case	Description
$\mu^{ji} = 0$	Component j does influence the degradation behavior of component i
$\mu^{ji} = 0$ and $\mu^{ij} = 0$	Component j and i are independently subject to gradual wear
$\mu^{ji} > 0$ and $\sigma^{ji} = 0$	Degradation evolution of component j does not depend on the state of component i

The effect of component j on component i does not have be to the same as the effect of component i on component j. The square hollow matrices

$$\mu^{ji} = \begin{pmatrix} 0 & \mu^{12} & \dots & \mu^{1n} \\ \mu^{21} & 0 & \dots & \mu^{2n} \\ \vdots & \vdots & 0 & \vdots \\ \mu^{n1} & \dots & \dots & 0 \end{pmatrix}, \ \sigma^{ji} = \begin{pmatrix} 0 & \sigma^{12} & \dots & \sigma^{1n} \\ \sigma^{21} & 0 & \dots & \sigma^{2n} \\ \vdots & \vdots & 0 & \vdots \\ \sigma^{n1} & \dots & \dots & 0 \end{pmatrix} \tag{5}$$

of size $n_c \times n_c$ can be used to represent these interactions.

These hollow matrices can be extended so that the diagonal entries are μ^{ii} and σ^{ii} respectively, representing the intrinsic wear effect of the components upon themselves; i.e. whereby the wear-rate of a component might depend on the wear level of the component itself, for example when the protection coating of a components fades Leyland & Matthews (2000).

In principle, this model can accommodate as many components and interactions as required. However, data, computation and the complexity of an optimal CBM policy are limitations. This is an identified issue in the multi-component maintenance literature Alaswad & Xiang (2017).

The parameters of the model must be estimated, about which there is a large literature, see for example An et al. (2015); Gebraeel & Pan (2008); Lorton et al. (2013). In practice, if the wear model is not too complicated, parameters may be estimated using maximum likelihood estimation (MLE). However, to do real-time prognostics for multi-component systems, it is recommended to use sequential Monte Carlo methods, specifically the particle filter (PF) Doucet & Johansen (2009).

We therefore use PF for performing parameter estimation of this model. PF has been applied successfully in prognostics, see e.g. Jouin et al. (2016). Moreover, recent reviews on PF for PHM such as Jouin et al. (2016) indicate the increasing use of PF in PHM, establishing it as a state-of-the-art technique for PHM.

Following the estimation of the parameters of the model, simulations are used to predict the health-state of a component $X^i_{t_k}$ at a future time $r > k$ and to determine t_{eol} as the time when the wear trajectory hits the failure threshold. Then the remaining-useful-life can be extracted, and maintenance decision-making follows accordingly.

3 EXTRACTING HEATH-INDICATORS FOR SYSTEMS WITH WEAR INTERACTIONS

Raw condition monitoring data have to be processed and refined to allow for health-indicator extraction for components. This is essential for performing prognostics in an effective manner, and so health-indicator extraction sits at the heart of any PHM framework.

Typically, measured signals from real systems are noisy Tandon & Choudhury (1999); Wang et al. (2003). Therefore, signal pre-processing and processing are necessary steps in health-indicator extraction (Figure 4). The signal pre-processing step aims to increase the signal-to-noise ratio (SNR). The signal processing step extracts health-indicators or fault-related information Lei et al. (2013, 2014) that allow accurate diagnosis and prediction of the future states of the system.

3.1 Data acquisition

As indicated in Figure 4, the first step is data acquisition from sensors, specifically accelerometers that measure vibration, which are commonly used for monitoring rotating machinery, e.g. gears Lebold et al. (2000), bearings An & Jiang (2014); Tandon & Choudhury (1999) and induc-

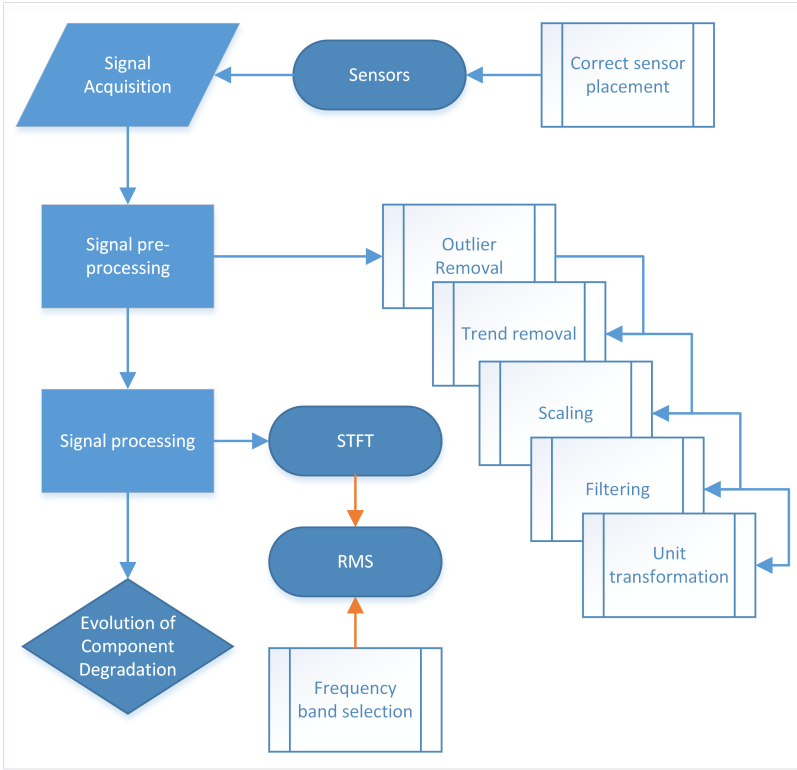

Figure 4 – Approach for extracting the health-state indicators of components in a multi-component system with wear interactions.

tion motors Benbouzid (2000). In a multi-component system setting, it is sensible to use multiple accelerometers. These accelerometers should not be positioned too close together, to allow separation of component signals. This is especially important when monitoring components which emit signals at similar frequencies.

3.2 Signal pre-Processing

Following data acquisition, a pre-processing step is typically used because clean data are not often found in an industrial setting. Thus, first cleaning the data specifically for outliers is advised. This is potentially a tedious manual task, and so we suggest the use of Algorithm 1, which is suitable for automation. This algorithm specifies a data-window based on the operating profile of the system. Then the median value or geometric mean of the data and the median absolute deviation (MAD) are computed over the window. Values that are outside the interval defined by the median +/- MAD are replaced with a random variable sampled as $X \sim \mathcal{N}(med,\ mad)$, thus retaining as much as possible of the true nature of the signal.

Algorithm 1: Outlier Removal Algorithm

w represents the window length;
input : A signal *Sig*, a row matrix of size $m \times w$
output: Signal *Sig* with no outliers

for $i \leftarrow 1$ **to** m **do**
  med←ComputeMedian($Sig(i)$);
  mad←ComputeMAD($Sig(i)$);
  for $j \leftarrow 1$ **to** w **do**
    if $Sig(i,j) < (med - mad)$ *or* $Sig(i,j) > (med + mad)$ **then**
      $Sig(i,j) = X \sim \mathcal{N}(med,\ mad)$
    end
  end
end

This should be followed by data detrending and centering. The data should also be rescaled if necessary, depending on whether sensors are dissimilar or if the data have different ranges. Filtering may follow this step, depending on the frequency band of interest and whether other unnecessary frequencies can be rejected without loss of information. Finally, the signal should be expressed in a unit that has an engineering meaning. This will depend on the specifics of the sensors. For example, if the sensors are accelerometers, then it is sensible to output the signal in units of gravitational acceleration (G).

3.3 Signal processing

Next, signal processing is used to extract features that represent health-state. A major challenge for modeling stochastic dependence in a multi-component system, if it exists, is the complex nature of the signals acquired. Each signal may be a mixture of the signals from each of the components at once, and the mixture may be different for each signal. Therefore, we recommend to use time-frequency domain analysis to obtain component-specific wear information from the signals of multi-component systems.

Time-frequency analysis is used in blind-source separation Abrard et al. (2001); Yilmaz & Rickard (2004). This separates mixed signals without using additional information by exploiting the difference in the time-frequency signatures of the signals. The main focus of the literature is audio applications Puigt & Deville (2005) and machine sound signals Zhong et al. (2006). Applications to vibration monitoring can be found in Dekys et al. (2017); Vulli et al. (2009).

Following this approach, a short-time Fourier transform (STFT) is applied to the cleaned signal, allowing an analysis in both time and frequency domains. This isolates the frequencies of interest all while representing the evolution of their energy through time.

Given the time-waveform data of a component i, the STFT can be applied using:

$$s_i^{'} = STFT\{s_i[n]\}(\tau,\omega) = \sum_{n=-\infty}^{+\infty} h[n-\tau]s[n]\exp^{-j\omega n} \tag{6}$$

Here $h(t)$ is the window function, $s(t)$ the input signal, and $s^{'}$ is the STFT of $s(t)$. The optimum window length depends on the application. It is important to note that a high resolution in time cannot be achieved simultaneously with a high resolution in frequency. A high resolution in time domain requires a shorter window than high resolution in the and vice-versa Kadambe (1992); Satish (1998). Therefore, to resolve the fundamental and harmonics of a signal, a long window is recommended. If the detection of the onset or presence of some events is prioritized then a short window should be used. Some examples of window functions are Gaussian and Hamming windows Harris (1978); Jones & Baraniuk (1994).

Following the STFT step, we can compute the frequency root mean square (FRMS) considering a frequency band of interest. This estimates the evolution in time of the magnitude of the frequency band of interest, and is calculated using:

$$X_{FRMS} = \sqrt{\frac{1}{N}\sum_{i=1}^{N} s_i^{'2}} \tag{7}$$

where N is the number of data points.

This results in time series signals that describe the evolution of the health condition of the components over time.

4 EXPERIMENTAL PLATFORM AND SCENARIOS

4.1 Existing platforms

In the literature on condition monitoring, two experimental platforms and their associated datasets stand out: the NASA bearing data Jay et al. (2007); Qiu et al. (2006); and the PRONOSTIA dataset Nectoux et al. (2012). They are very often cited in research on PHM and CBM. The former relates to three tests to failure of four bearings placed on a single shaft. The latter relates to an experimental platform for accelerated life testing of bearings and was used to generate the dataset for the IEEE ICPHM 2012 data challenge.

However, these experimental platforms do not provide datasets that are fit for the study of the wear interactions in multi-component systems. In particular, in the NASA dataset, when a fault is identified all components are then replaced. This does not allow the validation of interactions between components. Therefore we have developed a gearbox-platform 5 for the validation of models of wear of multi-component systems with stochastic dependence. The choice of a gearbox-platform is motivated by i) the multi-component nature of a gear-train, and ii) the common use of gearboxes in industrial machinery.

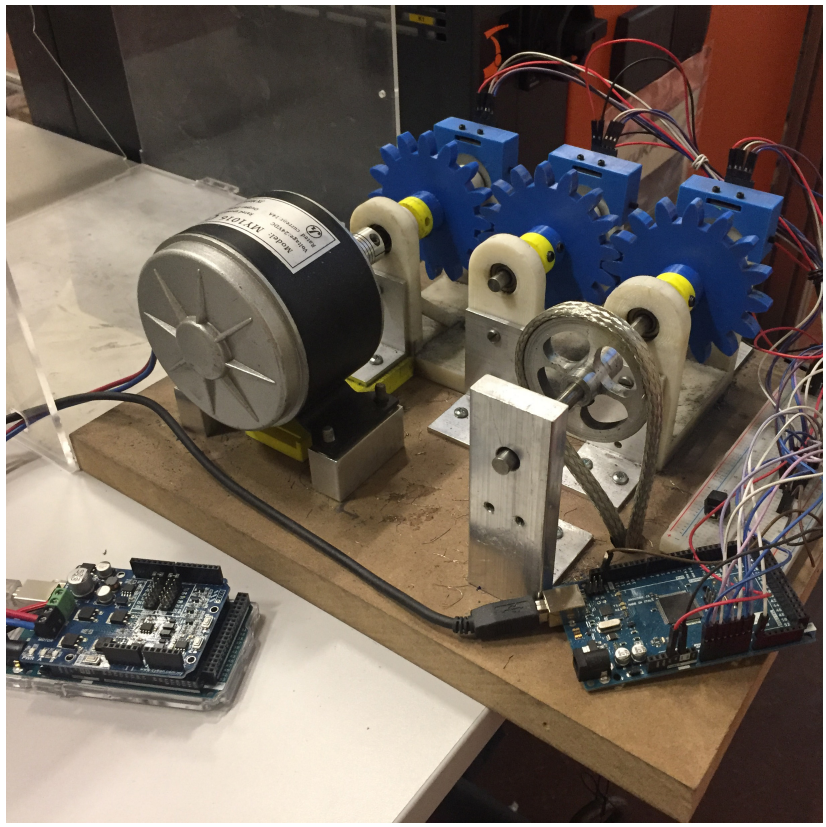

Figure 5 – Experimental gearbox-platform.

4.2 Description of the experimental platform

The platform was designed using computer aided design and 3D printing. It is re-configurable: gear modules of various materials, sizes and tooth-number can be tested. Other experimental parameters are adjustable: drives, loading and measurement devices, see Table 2.

The platform can have up to three gears mounted in series as shown in Figure 5, each mounted on its own shaft, using a frictionless rotation system. For this work however we study in detail the wear of two of these three gears. The gear directly connected to the motor is referred to as Gear

Table 2 – Experimental platform adjustable parameters.

Gears	Driving Part	Load Part	Measurements Part
Material	Motor type	Dynamometer brake	Accelerometers
Module	Torque	DC generator	Acoustic
	Speed	Pneumatic brake	DAQ specifications

1, and the other gear (the middle one) is referred to as Gear 2. The driving motor is a 24 Volt, 250 Watt motor capable of 2750 RPM. Full details of the platform are given in Assaf (2018).

We use three accelerometers, mounted on the frame, one over each shaft to collect vibration data. In this way the vibration signals for each of the gears under study can be more accurately distinguished. The accelerometer signals were collected using a DAQ and then transmitted to the processing workstation. The accelerometer sensors have a full sensing range of $\pm 3Gs$, and collect data along three axis. These are mounted over the centerline of the shaft supporting bearing to further avoid distortion of the vibration signals.

Digital data are imported to the processing workstation. Binary communication is used to ensure reliable data transmission. Sensor data are time-stamped using the DAQ internal microsecond clock, providing robust sampling time and sampling frequency.

4.3 Experimental scenario

As mentioned earlier, in this work we only mount two gears into the gearbox platform. We use this two-gear system in order to demonstrate stochastic dependence between components. The experimental runs of the gearbox are designed for accelerated-life testing, so that gears would degrade more rapidly than under normal operating conditions. Runs were an alternating sequence of two cycles: a low speed, low load cycle (LSLL); and a high speed, high load cycle (HSHL). There was a high noise level in the HSHL cycle, so only vibration data from an LSLL cycles were analyzed. These have a better signal to noise ratio. Thus, the platform was configured with alternating cycles of HSHL and LSLL. Each HSHL cycle was 9 minutes, and each LSLL cycle was 3 minutes.

The gearbox-platform was run three times to failure. In the first run, Run 1, Gear 1 and Gear 2 were both new and alternating HSHL and LSLL cycles continued until high levels of vibration and displacement were observed. A long enough exposure to such displacement can lead to a failure of the system structure. At this stage the measured vibration magnitude at the gear-meshing frequency exceeded 1800 in LSLL. We therefore consider this to be the experimental-run stopping criteria. After Run 1, Gear 1 was replaced, and Gear 2 remained unchanged. Thus, for Run 2, Gear 1 was new and Gear 2 was worn. Otherwise, the parameters were the same as Run 1. The gear-meshing frequency reached a magnitude of 1800 sooner and Gear 2 showed more damage on its teeth surface than after the termination of Run 1. After Run 2, Gear 1 was again replaced and Gear 2 remained unchanged. Thus, for Run 3, Gear 1 was new and Gear 2 was severely worn, otherwise experimental conditions and the stopping criteria remained the same.

4.4 Component health-state Extraction

In Figure 6 we show a two second sample extracted from Run 1. Here we visualize the raw signals following analogue to digital conversion. The signals were analyzed for outliers that may arise from transmission of the signal between the DAQ and the PC workstation. The data were then

centered and transformed to units of Gs (Figure 7). Next, the time waveform vibration signals were transformed into the time-frequency domain using STFT (Figure 8).

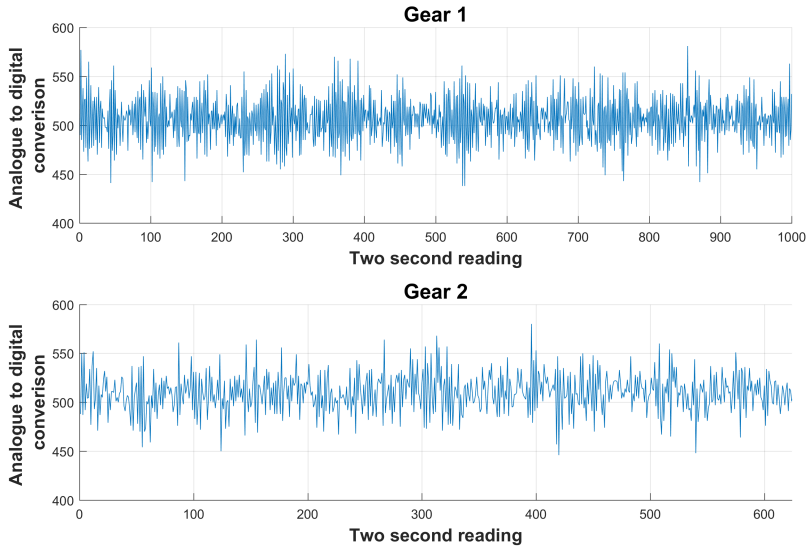

Figure 6 – Raw accelerometer signals of Gears 1 and 2 after the analogue to digital conversion.

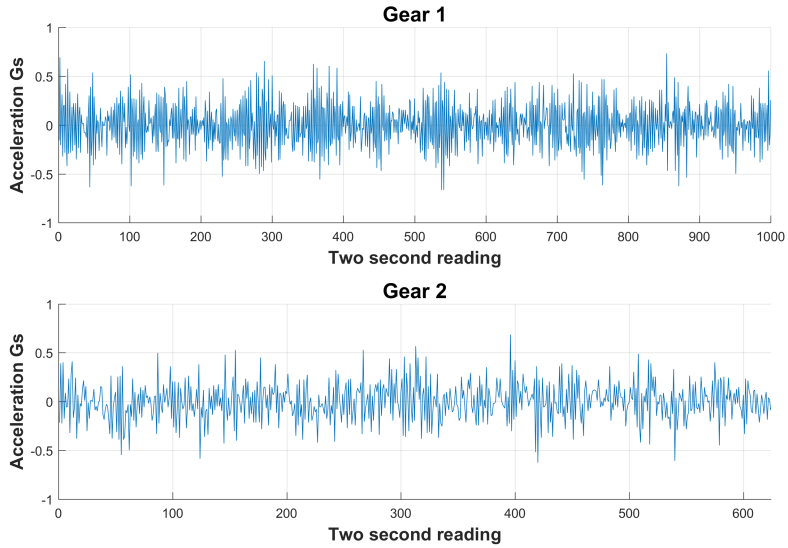

Figure 7 – Pre-processed accelerometer signals of Gears 1 and 2, in Gs.

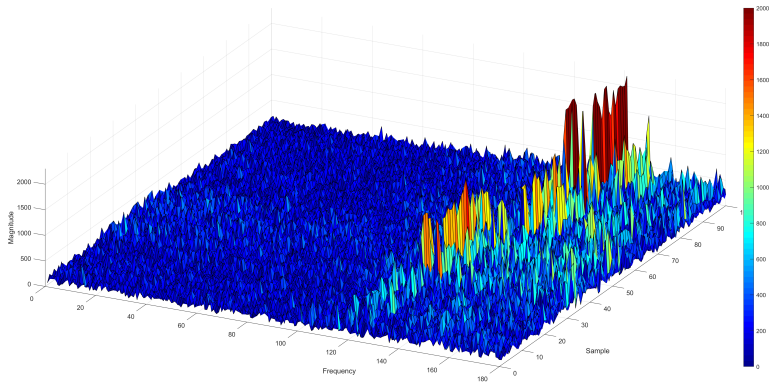

Figure 8 – Visual representation of the spectrum of frequencies of Gear 1 in Run 1 over time.

We then computed the average SNR of the signal to be 10.6 dB using equations:

$$SNR_{dB} = 10\log_{10}(\frac{P_{signal}}{P_{noise}}) \tag{8}$$

Then, we are interested to monitor the evolution of the gear meshing frequency magnitude f_{mesh} over time. This is computed as:

$$f_{mesh} = R \times N \tag{9}$$

where R is the revolutions per minute, and N is the number of teeth (here 16).

Due to a slight fluctuation in the motor speed that affected f_{mesh}, we used dynamic-windowing to capture f_{mesh}, choosing a 5Hz frequency band that is guaranteed to contain f_{mesh} at its peak magnitude. We then calculated the RMS at that frequency band, and monitored its evolution over time. f_{mesh} was 120Hz approximately. Thus, here we use the fundamental meshing frequency (120 Hz) to assess the health-state of the gears. We can therefore remove all frequency elements that are greater that this value without affecting the information about the frequency of interest. We therefore specified a cutoff frequency of 180Hz for the high pass filter. This allows for faster computation and is justified because only the fundamental f_{mesh} frequency is of interest. Note that the specification of cutoff frequency requires engineering knowledge of the system at hand.

We then computed the RMS value for each time step, and the gear mesh frequency was normalized for the range $[0\ 1800]$. This resulted in the wear time series shown in Figure 12. Black dashed vertical lines separate the experimental runs. Silver dotted vertical lines separate data collection cycles, i.e. the LSLL cycles. Note that a) between every two LSLL cycles there exists an HSHL cycle, and b) HSHL cycles are not shown in this figure because vibration data from these cycles were discarded.

We specify a failure threshold L based on the experimental runs, the vibration signals emitted, and the different phases of wear that were observed on the gear tooth surfaces. The failure threshold

Table 3 – Average gear meshing frequency magnitude for each LSLL cycle for both gears in all three runs.

		LSLL Cycle Number									
Run	Gear	1	2	3	4	5	6	7	8	9	10
1	1	.283	.260	.257	.373	.230	.279	.183	.518	.735	.624
1	2	.347	.267	.325	.360	.253	.388	.283	.580	.560	.602
2	1	.314	.255	.366	.303	.606	.507				
2	2	.464	.465	.489	.477	.626	.604				
3	1	.358	.344	.507	.571						
3	2	.595	.490	.570	.667						

Table 4 – Cycles to first hitting time of Gear 1 at each run.

	Gear 1	Gear 2	Gear 1's cycles to failure	Gear 1's life expectancy (%)
Run 1	new	new	7	100
Run 2	new	worn	4	57
Run 3	new	severely worn	3	43

L corresponds to the gear meshing frequency magnitude 0.65. At this threshold the gearbox-platform emits high levels of vibration and displacement, with potential for damage to the system structure as a whole. The system is therefore stopped, and we consider this as a system failure.

Next, we computed the average of each LSLL cycle to show the wear interactions between the gears (Table 3). Note that the average meshing frequency magnitude does not necessarily increase at every LSLL cycle. This small fluctuation is due to the distortion of the signal acquired by the accelerometers when changing between HSHL and LSLL cycles. Another thing to consider is that wear on the teeth of the gears such as pitting and dents can cause transient higher vibration. These are damped when the surface of the tooth becomes relatively smoother during operation. Nevertheless, we can see that there is a general increasing trend in vibration as the LSLL cycle count increases, indicative of wear of the gears.

Wear interactions are apparent in Table 3. However, this is clearer in Table 4, here the cycles to failure are evaluated as the number of cycles to first hitting time, i.e. when the moving average of the signal first reaches L. We see that the number of cycles to first hitting time for Gear 1 is shorter when Gear 2 is worn (at Run 2) than when Gear 2 is new (at Run 1). And it is most short when Gear 3 is severely worn (at Run 3). Thus, coupling a new component with a worn-out component has resulted in accelerated wear of the new component at each step.

These results clearly demonstrate the importance of modeling wear interaction between gears when performing prognostics for a multi-component system. Thus, if one replaces a specific component in the system with a new one, ignoring the accelerated wear effect that results from its being coupled with a worn component, there would arise unexpected failures and faults because the new component(s) would not degrade in nominal fashion.

5 IMPLEMENTATION OF THE GAUSSIAN MIXTURE MODEL BASED DIAGNOSTICS

5.1 Clustering of different wear phases

Wear of two gear components is clustered in two dimensions. These dimensions are the wear-state of Gear 1 and the wear-state of Gear 2. We use the magnitude of the RMS gear mesh frequency to represent component wear. These wear data are obtained from Run 1. The clustering algorithm is repeated ten times, to check for sensitivity to starting conditions. Each repetition has 200 EM steps. We use a diagonal matrix for the GMM as this is computationally faster than for a general covariance matrix, which allows more frequent updating of clusters. Also, for flexibility in the range of the clusters, different covariance matrices are not used for different clusters.

Using the silhouette analysis, and considering a cluster count between 3 and 6, the optimal cluster count is found to be 3 in our case. The silhouette plot for 3 clusters is shown in Figure 9. It presents the highest average silhouette value for all clusters which suggests that clustering using three clusters is appropriate.

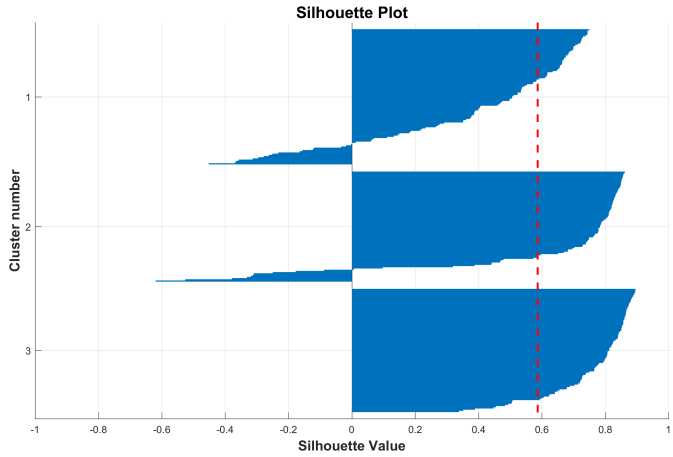

Figure 9 – Silhouette plot for three clusters with the dashed red line is the average silhouette value for all three clusters

The result of clustering (for the wear in experimental Run 1) is shown in Figure 10, showing the three clusters with their corresponding bivariate Gaussian distributions.

The plot suggests that the clusters represent different stages of wear: a healthy state (green), a defective state (blue); and a worn-out state (red).

5.2 Diagnostics results

Having partitioned the wear in Run 1 into three clusters, we can use the clustering model to classify new datapoints. This is the basis for diagnosis of the system. We demonstrate this next

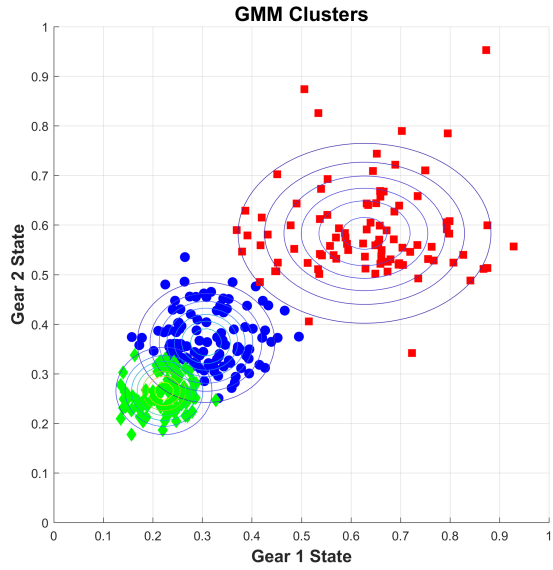

Figure 10 – Wear from experimental Run 1 with three clusters.

for Runs 2 and 3. (Figure 11). There the wear trajectories are overlaid with the cluster assignment. We can see that initially in Run 2 wear data points are assigned to blue cluster (defective). Initially in Run 3, they are assigned to the red cluster (worn-out). This because Gear 1 fails sooner in Run 2 than in Run 1 and sooner again in Run 3 than in Runs 1 and 2. This was as expected because only Gear 1 was replaced immediately prior to the commencement of experimental Runs 2 and 3. Thus, we can conclude that these clusters not only represent the wear-states of the system, but their wear-rates. Therefore, three wear phases can be identified for this multi-component system.

6 IMPLEMENTATION OF THE PARTICLE FILTER BASED PROGNOSTICS

6.1 Parameter estimation

The proposed generic multi-component wear model is fitted to the data generated from the gearbox-platform. Following the health-indicator extraction step, we obtain the RMS trajectories for Gear 1 and Gear 2 (Figure 12).

The RMS values represent the vibration energy in the machine that derives from the gears. Hence, the RMS values represent the wear level of the gears because the higher the vibration energy, the more the gears are deteriorated and the more prone the gearbox is to damage. Indeed, the increasing damage of a gear i ($i = 1,2$) in reality derives from the gear state (intrinsic effect ΔX_t^{ii}) and the state of the other gear (interaction effect ΔX^{ji} with $j \neq i$). This is because both gears are subject to wear and have a direct connection. Based on the results of Section 4, a gear

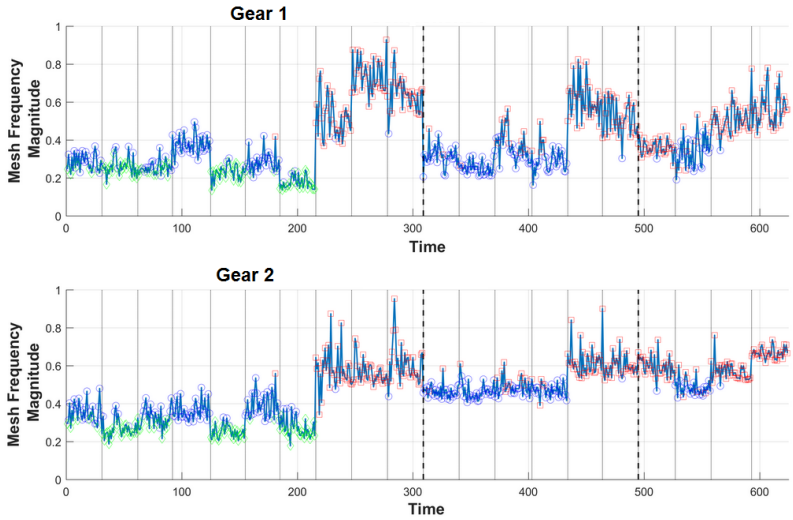

Figure 11 – Wear phases overlaid on the time series wear data of the two gears from 3 experimental runs.

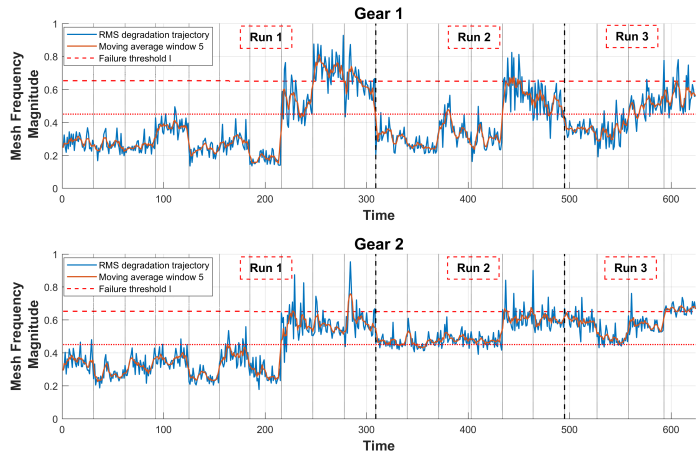

Figure 12 – RMS wear trajectories for Gears 1 and 2.

is considered to be severely worn or failed when its wear level reaches the threshold vibration magnitude of $L^i = 0.65$ for $i = 1, 2$.

The wear process of each gear is assumed to be described by a gamma distribution:

$$X \sim \Gamma(\alpha^i, \beta^i).$$

The corresponding probability density function (PDF) is

$$f_{\alpha^i,\beta^i}(x) = \frac{1}{\Gamma(\alpha^i)}(\beta^i)^{\alpha^i} x^{\alpha^i - 1} e^{-\beta^i x} \mathscr{I}_{\{x \geq 0\}},$$

where $\Gamma(\alpha^i) = \int_0^{+\infty} u^{\alpha^i - 1} e^{-u} du$ denotes the gamma function; and $\mathscr{I}_{\{x \geq 0\}}$ is an indicator function. $\mathscr{I}_{\{x \geq 0\}} = 1$ if $x \geq 0$, $\mathscr{I}_{\{x \geq 0\}} = 0$ and otherwise.

These increments are denoted by ΔX^{11} and ΔX^{22} for Gear 1 and Gear 2 respectively. Thus, $\Delta X^{11} \sim \Gamma(\alpha^1, \beta^1)$ and $\Delta X^{22} \sim \Gamma(\alpha^2, \beta^2)$.

Concerning the wear interactions between the two gears, Figure 12 shows that that the wear-state of Gear 2 affects the wear-rate of Gear 1. This can be seen clearly by observing the time to failure of Gear 1 when coupled with a worn Gear 2 in both Runs 2 and 3. Further, in Run 3, where Gear 2 was severly worn, the time to failure of Gear 1 was shorter than in Run 2. Thus, it appears that the wear-rate of Gear 1 depends on the wear level of Gear 2 and vice versa. This is further studied in Section 5. We model the wear interactions between the two gears using Equation (4).

Finally, the evolution of wear for Gear 1 can be expressed as:

$$\begin{aligned} X_t^1 &= X_{t-1}^1 + \Delta X_t^1, \\ \Delta X_t^1 &= \Delta X^{11} + \Delta X^{21}, \\ \Delta X_t^1 &= \Gamma(\alpha^1, \beta^1) + \mu^{21} \times (X_{t-1}^2)^{\sigma^{21}}. \end{aligned} \tag{10}$$

and for GEAR 2 as:

$$\begin{aligned} X_t^2 &= X_{t-1}^2 + \Delta X_t^2, \\ \Delta X_t^2 &= \Delta X^{22} + \Delta X^{12}, \\ \Delta X_t^2 &= \Gamma(\alpha^2, \beta^2) + \mu^{12} \times (X_{t-1}^1)^{\sigma^{12}}. \end{aligned} \tag{11}$$

According to the above models, for each gear i ($i = 1, 2$) four parameters $(\alpha^i, \beta^i, \mu^i, \sigma^i)$ need to be estimated from the recorded data.

For each set of parameters, selected at random from a prior distribution, we generate $n_p = 1000$ particles,. We then generate a prediction of the health state at the next time step, $\tilde{X}_t^{i,n}$ for $n = 1 : n_p$. On observing the actual health state at the next time step, y_t^i, we compute the importance (weight) of each particle as the likelihood of the observation given the predicted values of each particle $p(y_t | \tilde{X}_{t+1}^{i,n})$. The weights are then normalized, and bootstrap-importance sampling (re-sampling with replacement according to weight) is used to generate the next set of n_p particles. This process iterates until reaching the last time step.

Parameter estimates are in Table 5. Note, larger values of σ^i imply smaller effects of the other components on component i because the wear level is normalized between 0 and 1.

To further validate these parameter estimates, we compare the average estimated wear trajectory resulting from the PF to the real wear trajectories using R^2: for component 1, $R_1^2 = 0.792$ and for component 2 $R_2^2 = 0.753$. In a model without wear interaction (stochastic dependence), the corresponding results are $R_1^2 = 0.671$ and $R_2^2 = 0.575$.

Figure 13 shows the particle filter fit to the wear data of Run 1 for each component. Herein, silver dots are the estimated wear levels at each time step corresponding to each of the n_p particles. The

Table 5 – Estimated parameter values.

Component	α^i	β^i	μ^i	σ^i
Gear 1	0.0233	0.0425	0.0995	7.6659
Gear 2	0.0125	0.0914	0.0493	9.7375

yellow dashed line is the average of these n_p estimates of wear. A moving average of window of width five (green line) smooths the observed wear trajectory and provides an effective indication that a gear has failed once it reaches the failure threshold L.

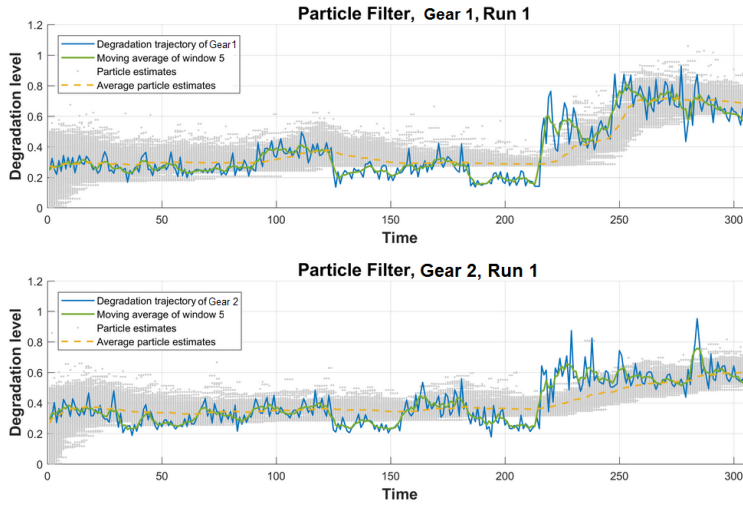

Figure 13 – Fit of particle filter estimates to wear data of Gears 1 and 2.

6.2 End-of-life prediction for gears

The wear model with the estimates in Table 5 is used to predict the end-of-life of each gear by generating a large number of wear trajectories. To study the impact of wear interaction between gears in predicting the end-of-life of gears, two cases are specified: ”With Interaction” whereby the wear trajectories are generated from Equations (10) and (11); ”No Interaction” whereby the wear trajectories are generated from the reduced model in which there is no wear interaction.

Figures 14 and 15 show different wear trajectories for Gear 1 and Gear 2 in Run 1. Since only Gear 1 is replaced for Runs 2 and 3 (Gear 2 remains unchanged), only the wear process of Gear 1 is generated in Run 2 and 3 (see Figures 16 and 17).

Intuitively, the simulated results show that considering wear dependencies can provide an advantage when attempting to predict the real wear trajectories of gears.

Table 6 reports the different t_{eol} estimates. These results show that the difference between the actual observed t_{eol} and the average predicted $\widehat{t}_{eol}$ for Gear 1 when not considering the wear

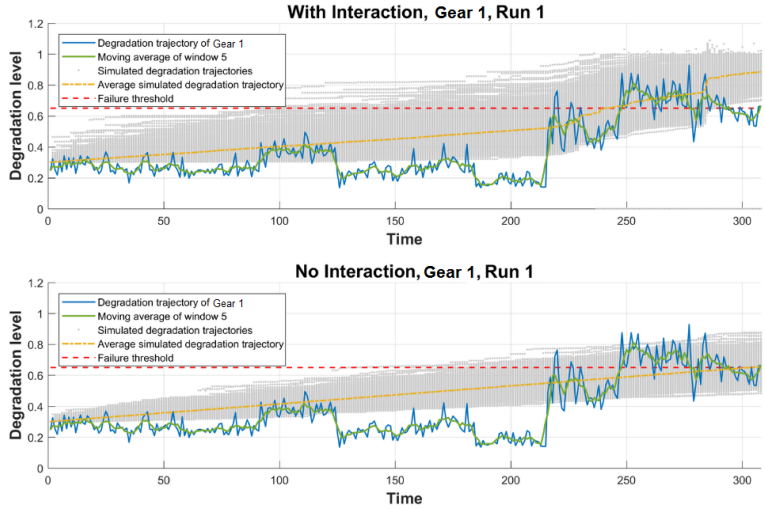

Figure 14 – Simulated wear trajectories for Gear 1 in Run 1.

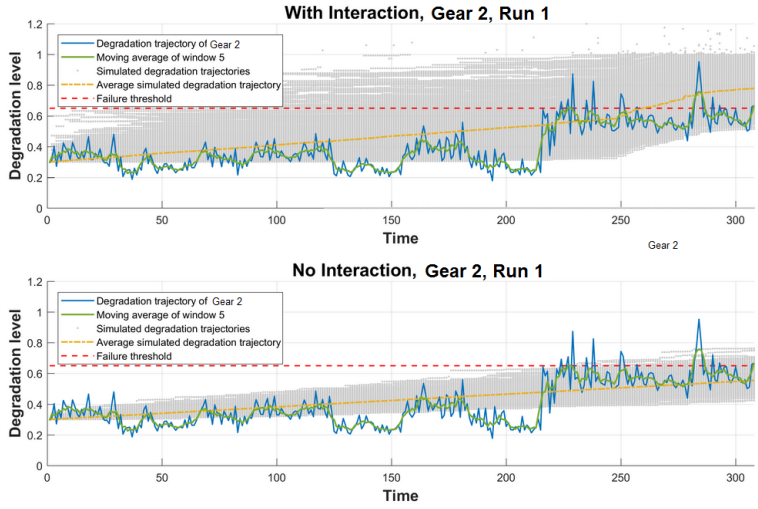

Figure 15 – Simulated wear trajectories for Gear 2 in Run 1.

Table 6 – Actual end-of-life, and average predicted end-of-life ($\widehat{t_{eol}}$) for the two gears.

	Actual t_{eol}		$\widehat{t_{eol}}$ with interaction		$\widehat{t_{eol}}$ no interaction	
	Gear 1	Gear 2	Gear 1	Gear 2	Gear 1	Gear 2
Run 1	248	227	239	259	301	429
Run 2	133	faulty	157	faulty	301	faulty
Run 3	111	faulty	118	faulty	301	faulty

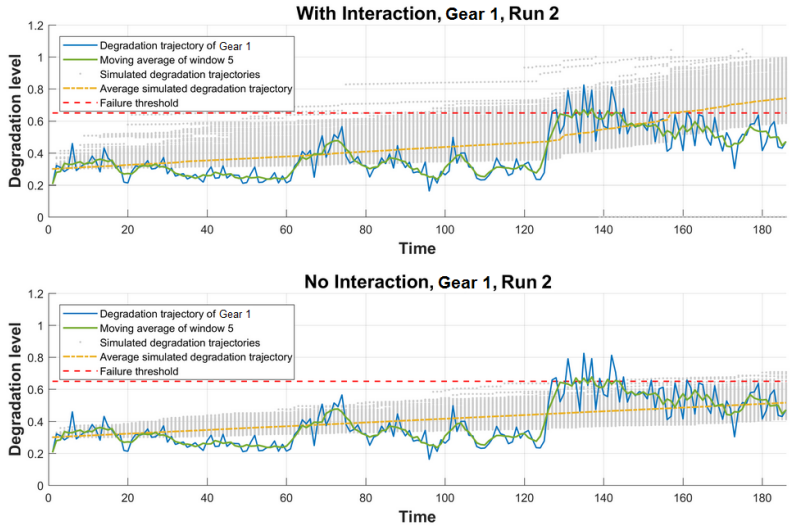

Figure 16 – Simulated wear trajectories for Gear 1 in Run 2.

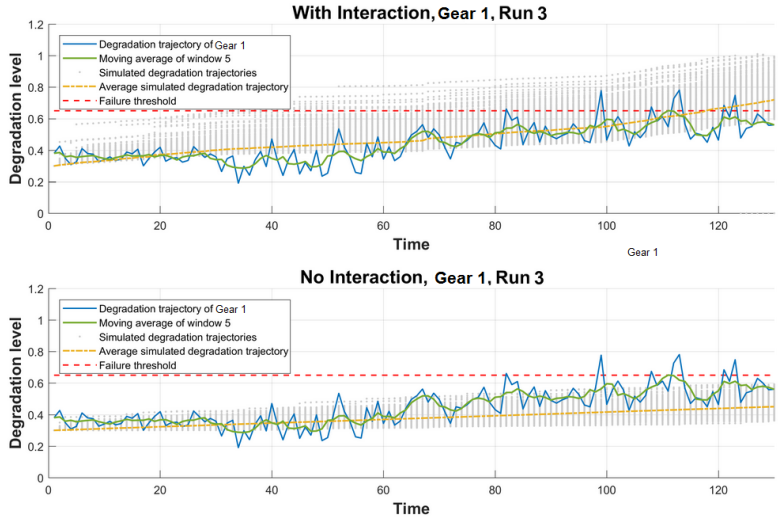

Figure 17 – Simulated wear trajectories for Gear 1 in Run 3.

interaction shows a strict growth trend. Indeed, this growth begins at time step 53 in Run 1, and continues to time step 168 in Run 2, and then 190 in Run 3. The explanation for this difference is that the parameters of the models are estimated in Run 1 using the particle filter (PF) and so the reduced model does not account for the accelerated wear due to a new Gear 1 being coupled with a worn Gear 2. Furthermore, the difference does not show this trend when we consider the wear

interaction (stochastic dependence). The difference is 9 in Run 1, then 24 in Run 2, and then just 7 in Run 3. This shows the importance of modeling the wear interaction.

In addition, histograms simulated from the estimated wear distributions at the time of failure of the gears are shown in Figures 18 and 19.

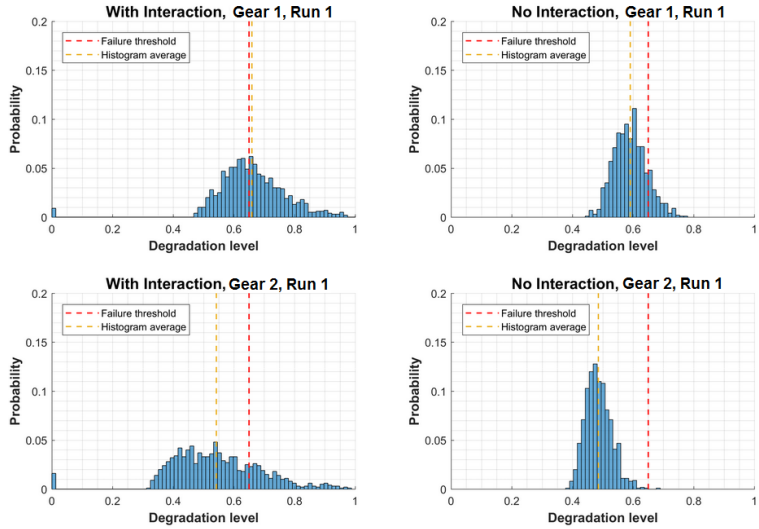

Figure 18 – Histograms of the estimated wear distributions at the actual end-of-life of Gears 1 and 2 in Run 1.

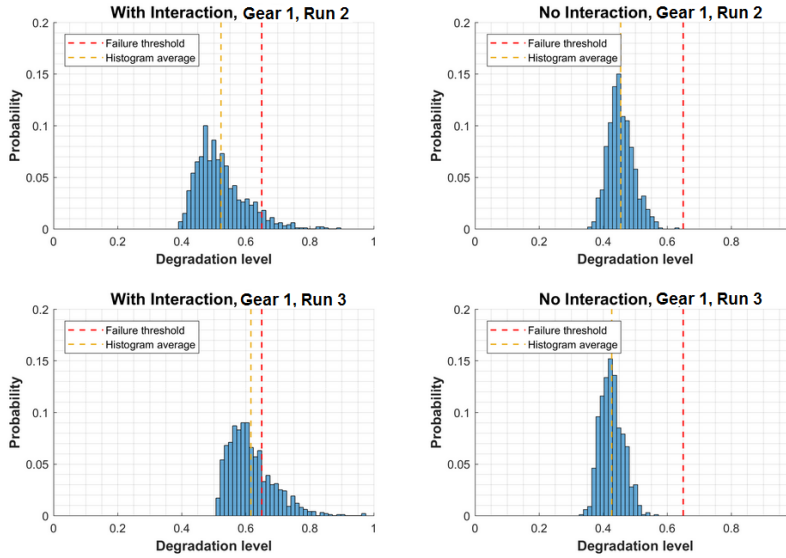

Figure 19 – Histograms of the estimated wear distribution at the actual time to end-of-life of Gear 1 in Runs 2 and 3.

These again suggest that modeling stochastic dependence impacts upon the prediction of the actual wear trajectories since the average estimated wear level is closer to the failure threshold when wear interaction is considered than when it is not.

Finally, note, these predictions of t_{eol} are simulated at $t = 0$ in Runs 2 and 3. Therefore, if particle filtering is used for online updating of parameters in presence of new observations (of wear), prediction accuracy would increase. This would also facilitate the investigation of break points in the health-state of gears, due to shocks arising from changes in the environment or sudden excess loading, for example.

7 CONCLUSION

In this paper we present a framework for diagnostics and prognostics for multi-component systems with stochastic dependence between components. The proposed framework is applied to data generated on an experimental gearbox-platform. We demonstrate how to extract health-indicator information from such systems. These indicators are then used to perform diagnostics that help to identify three wear phases for the system, each having a different wear-rate. We follow this with a prognostics approach that uses particle filtering and a generic multi-component wear model. We present a comparative study of a model in which stochastic dependence is considered and a reduced model in which it is not. Our results indicate that modeling stochastic dependence provides more accurate predictions of the end-of-life of components, and hence remaining-useful-lives, and so provides a better basis for PHM and maintenance decision making.

In future work we intend to focus on the development of a system to automate predictive maintenance optimization for multi-component systems with rate-state wear interactions. For this we foresee the development of an emulator of the wear of components in a multi-component system with wear interactions between components. The basis of such an emulator would be data collected on an experimental platform such as the one we describe. Using the emulator, many realizations of multi-variate wear trajectories could be simulated under varying replacement policies. Then, an autonomous system could learn those policies that are most effective. Some additional randomness might be introduced to the emulator to capture unforeseen circumstances.

Finally, we comment on the limitations of the work we describe in this paper. The raw vibration data are rather noisy. With hindsight we would design a gearbox emulator with gears with more varied characteristics, position accelerometers more carefully, and significantly over-specify bearings, the motor, and the loading and energy dissipation devices. Also, other more direct wear-related variables, such as tooth profile and gear backlash, might be measured optically. Nonetheless, we think the experimental platform, the condition data obtained from it, and the analysis of these data make an important contribution to the study of PHM for systems with wear rate-state interactions.

References

ABRARD F, DEVILLE Y & WHITE P. 2001. A new source separation approach based on time-frequency analysis for instantaneous mixtures. *Proc. ECM2S*, pp. 259–267.

ALASWAD S & XIANG Y. 2017. A review on condition-based maintenance optimization models for stochastically deteriorating system. *Reliability Engineering & System Safety*, **157**: 54–63.

AN D, KIM NH & CHOI JH. 2015. Practical options for selecting data-driven or physics-based prognostics algorithms with reviews. *Reliability Engineering & System Safety*, **133**: 223–236.

AN X & JIANG D. 2014. Bearing fault diagnosis of wind turbine based on intrinsic time-scale decomposition frequency spectrum. *Proceedings of the Institution of Mechanical Engineers, Part O: Journal of Risk and Reliability*, **228**(6): 558–566.

ASSAF R. 2018. *Prognostics And Health Management For Multi-component Systems*. Ph.D. thesis. University of Salford.

ASSAF R, DO P, NEFTI-MEZIANI S & SCARF P. 2018. Wear rate–state interactions within a multi-component system: a study of a gearbox-accelerated life testing platform. *Proceedings of the Institution of Mechanical Engineers, Part O: Journal of Risk and Reliability*, **232**(4): 425–434.

ASSAF R, DO P, SCARF P & NEFTI-MEZIANI S. 2016. Wear rate-state interaction modelling for a multi-component system: Models and an experimental platform. *IFAC-PapersOnLine*, **49**(28): 232–237.

BENBOUZID MEH. 2000. A review of induction motors signature analysis as a medium for faults detection. *IEEE Transactions on Industrial Electronics*, **47**(5): 984–993.

BIAN L & GEBRAEEL N. 2014. Stochastic framework for partially degradation systems with continuous component degradation-rate-interactions. *Naval Research Logistics (NRL)*, **61**(4): 286–303.

BOUVARD K, ARTUS S, BÉRENGUER C & COCQUEMPOT V. 2011. Condition-based dynamic maintenance operations planning & grouping. Application to commercial heavy vehicles. *Reliability Engineering & System Safety*, **96**(6): 601–610.

CELEUX G & GOVAERT G. 1995. Gaussian parsimonious clustering models. *Pattern recognition*, **28**(5): 781–793.

DASGUPTA A & RAFTERY AE. 1998. Detecting features in spatial point processes with clutter via model-based clustering. *Journal of the American Statistical Association*, **93**(441): 294–302.

DE JONGE B & SCARF PA. 2020. A review on maintenance optimisation. *European Journal of Operational Research*, **285**: 805–824.

DEKKER R, WILDEMAN RE & VAN DER DUYN SCHOUTEN FA. 1997. A review of multi-component maintenance models with economic dependence. *Mathematical Methods of Operations Research*, **45**(3): 411–435.

DEKYS V, KALMAN P, HANAK P, NOVAK P & STANKOVICOVA Z. 2017. Determination of vibration sources by using STFT. *Procedia Engineering*, **177**: 496–501.

DINH DH, DO P & IUNG B. 2020. Degradation modeling and reliability assessment for a multi-component system with structural dependence. *Computers & Industrial Engineering*, **144**: 106443.

DOUCET A & JOHANSEN AM. 2009. A tutorial on particle filtering and smoothing: Fifteen years later. *Handbook of Nonlinear Filtering*, **12**(656-704): 3.

FREI R, MCWILLIAM R, DERRICK B, PURVIS A, TIWARI A & SERUGENDO GDM. 2013. Self-healing and self-repairing technologies. *The International Journal of Advanced Manufacturing Technology*, **69**(5-8): 1033–1061.

FREITAS MA, COLOSIMO EA, SANTOS TRD & PIRES MC. 2010. Reliability assessment using degradation models: Bayesian and classical approaches. *Pesquisa Operacional*, **30**: 194–219.

GEBRAEEL N & PAN J. 2008. Prognostic degradation models for computing and updating residual life distributions in a time-varying environment. *IEEE Transactions on Reliability*, **57**(4): 539–550.

GRALL A, BÉRENGUER C & DIEULLE L. 2002. A condition-based maintenance policy for stochastically deteriorating systems. *Reliability Engineering & System Safety*, **76**(2): 167–180.

HAO H, ZHANG K, DING SX, CHEN Z & LEI Y. 2014. A data-driven multiplicative fault diagnosis approach for automation processes. *ISA transactions*, **53**(5): 1436–1445.

HARRIS FJ. 1978. On the use of windows for harmonic analysis with the discrete Fourier transform. *Proceedings of the IEEE*, **66**(1): 51–83.

HOSEINZADEH MS, KHADEM SE & SADOOGHI MS. 2018. Quantitative diagnosis for bearing faults by improving ensemble empirical mode decomposition. *ISA transactions*, **83**: 261–275.

JARDINE AK, LIN D & BANJEVIC D. 2006. A review on machinery diagnostics and prognostics implementing condition-based maintenance. *Mechanical Systems and Signal Processing*, **20**(7): 1483–1510.

JAY L, HAI Q, GANG Y, JING L & SERVICES RT. 2007. Bearing Data Set.

JIMENEZ JJM, SCHWARTZ S, VINGERHOEDS R, GRABOT B & SALAÜN M. 2020. Towards multi-model approaches to predictive maintenance: A systematic literature survey on diagnostics and prognostics. *Journal of Manufacturing Systems*, **56**: 539–557.

JONES DL & BARANIUK RG. 1994. A simple scheme for adapting time-frequency representations. *IEEE Transactions on Signal Processing*, **42**(12): 3530–3535.

JOUIN M, GOURIVEAU R, HISSEL D, PÉRA MC & ZERHOUNI N. 2016. Particle filter-based prognostics: Review, discussion and perspectives. *Mechanical Systems and Signal Processing*, **72**: 2–31.

KADAMBE S. 1992. On the window selection and the cross terms that exist in the magnitude squared distribution of the short time Fourier transform. In: *Statistical Signal and Array Processing, 1992. Conference Proceedings., IEEE Sixth SP Workshop on*. pp. 22–25. IEEE.

KEIZER MCO, FLAPPER SDP & TEUNTER RH. 2017. Condition-based maintenance policies for systems with multiple dependent components: A review. *European Journal of Operational Research*, .

KIM NH, AN D & CHOI JH. 2017. *Prognostics and Health Management of Engineering Systems*. Springer.

LEBOLD M, MCCLINTIC K, CAMPBELL R, BYINGTON C & MAYNARD K. 2000. Review of vibration analysis methods for gearbox diagnostics and prognostics. In: *Proceedings of the 54th meeting of the Society for Machinery Failure Prevention Technology*, vol. 634. p. 16.

LEI Y, LI N, LIN J & WANG S. 2013. Fault diagnosis of rotating machinery based on an adaptive ensemble empirical mode decomposition. *Sensors*, **13**(12): 16950–16964.

LEI Y, LIN J, HAN D & HE Z. 2014. An enhanced stochastic resonance method for weak feature extraction from vibration signals in bearing fault detection. *Proceedings of the Institution of Mechanical Engineers, Part C: Journal of Mechanical Engineering Science*, **228**(5): 815–827.

LEYLAND A & MATTHEWS A. 2000. On the significance of the H/E ratio in wear control: a nanocomposite coating approach to optimised tribological behaviour. *Wear*, **246**(1-2): 1–11.

LORTON A, FOULADIRAD M & GRALL A. 2013. A methodology for probabilistic model-based prognosis. *European Journal of Operational Research*, **225**(3): 443–454.

NECTOUX P, GOURIVEAU R, MEDJAHER K, RAMASSO E, CHEBEL-MORELLO B, ZERHOUNI N & VARNIER C. 2012. PRONOSTIA: An experimental platform for bearings accelerated degradation tests. In: *IEEE International Conference on Prognostics and Health Management, PHM'12.*. pp. 1–8. IEEE.

NGUYEN KA, DO P & GRALL A. 2014. Condition-based maintenance for multi-component systems using importance measure and predictive information. *International Journal of Systems Science: Operations & Logistics*, **1**(4): 228–245.

NGUYEN KT & MEDJAHER K. 2019. A new dynamic predictive maintenance framework using deep learning for failure prognostics. *Reliability Engineering & System Safety*, .

NICOLAI RP & DEKKER R. 2008. Optimal maintenance of multi-component systems: a review. In: *Complex System Maintenance Handbook*. pp. 263–286. Springer.

NICOLAI RP, FRENK JBG & DEKKER R. 2009. Modelling and optimizing imperfect maintenance of coatings on steel structures. *Structural Safety*, **31**(3): 234–244.

OUYANG M, WELSH WJ & GEORGOPOULOS P. 2004. Gaussian mixture clustering and imputation of microarray data. *Bioinformatics*, **20**(6): 917–923.

PENG Y, DONG M & ZUO MJ. 2010. Current status of machine prognostics in condition-based maintenance: a review. *The International Journal of Advanced Manufacturing Technology*, **50**(1-4): 297–313.

PUIGT M & DEVILLE Y. 2005. Time–frequency ratio-based blind separation methods for attenuated and time-delayed sources. *Mechanical Systems and Signal Processing*, **19**(6): 1348–1379.

QIU H, LEE J, LIN J & YU G. 2006. Wavelet filter-based weak signature detection method and its application on rolling element bearing prognostics. *Journal of Sound and Vibration*, **289**(4): 1066–1090.

RASMEKOMEN N & PARLIKAD AK. 2016. Condition-based maintenance of multi-component systems with degradation state-rate interactions. *Reliability Engineering & System Safety*, **148**: 1–10.

ROUSSEEUW PJ. 1987. Silhouettes: a graphical aid to the interpretation and validation of cluster analysis. *Journal of Computational and Applied Mathematics*, **20**: 53–65.

SATISH L. 1998. Short-time Fourier and wavelet transforms for fault detection in power transformers during impulse tests. *IEE Proceedings-Science, Measurement and Technology*, **145**(2): 77–84.

SATOW T & OSAKI S. 2003. Optimal replacement policies for a two-unit system with shock damage interaction. *Computers & Mathematics with Applications*, **46**(7): 1129–1138.

SAXENA A, CELAYA J, BALABAN E, GOEBEL K, SAHA B, SAHA S & SCHWABACHER M. 2008. Metrics for evaluating performance of prognostic techniques. In: *Prognostics and Health Management, PHM 2008. International Conference on*. pp. 1–17. IEEE.

SCARF P & DEARA M. 1998. On the development and application of maintenance policies for a two-component system with failure dependence. *IMA Journal of Management Mathematics*, **9**(2): 91–107.

TANDON N & CHOUDHURY A. 1999. A review of vibration and acoustic measurement methods for the detection of defects in rolling element bearings. *Tribology International*, **32**(8): 469–480.

THOMAS L. 1986. A survey of maintenance and replacement models for maintainability and reliability of multi-item systems. *Reliability Engineering*, **16**(4): 297–309.

VACHTSEVANOS GJ, LEWIS F, HESS A & WU B. 2006. *Intelligent fault diagnosis and prognosis for engineering systems*. Wiley Online Library.

VAN NOORTWIJK J. 2009. A survey of the application of gamma processes in maintenance. *Reliability Engineering & System Safety*, **94**(1): 2–21.

VULLI S, DUNNE J, POTENZA R, RICHARDSON D & KING P. 2009. Time-frequency analysis of single-point engine-block vibration measurements for multiple excitation-event identification. *Journal of Sound and Vibration*, **321**(3-5): 1129–1143.

WANG D, TSUI KL & MIAO Q. 2017. Prognostics and health management: A review of vibration based bearing and gear health indicators. *IEEE Access*, **6**: 665–676.

WANG J, LI R & PENG X. 2003. Survey of nonlinear vibration of gear transmission systems. *Applied Mechanics Reviews*, **56**(3): 309–329.

WANG X, JIANG B & LU N. 2019. Adaptive relevant vector machine based RUL prediction under uncertain conditions. *ISA transactions*, **87**: 217–224.

WU CJ ET AL. 1983. On the convergence properties of the EM algorithm. *The Annals of Statistics*, **11**(1): 95–103.

WU J, HU K, CHENG Y, ZHU H, SHAO X & WANG Y. 2019. Data-driven remaining useful life prediction via multiple sensor signals and deep long short-term memory neural network. *ISA transactions*, .

YAJIMA A, WANG H, LIANG RY & CASTANEDA H. 2015. A clustering based method to evaluate soil corrosivity for pipeline external integrity management. *International Journal of Pressure Vessels and Piping*, **126**: 37–47.

YAN M, WANG X, WANG B, CHANG M & MUHAMMAD I. 2019. Bearing remaining useful life prediction using support vector machine and hybrid degradation tracking model. *ISA transactions*, .

YEUNG KY, FRALEY C, MURUA A, RAFTERY AE & RUZZO WL. 2001. Model-based clustering and data transformations for gene expression data. *Bioinformatics*, **17**(10): 977–987.

YILMAZ O & RICKARD S. 2004. Blind separation of speech mixtures via time-frequency masking. *IEEE Transactions on Signal Processing*, **52**(7): 1830–1847.

ZHONG Z, CHEN J, ZHONG P & WU J. 2006. Application of the blind source separation method to feature extraction of machine sound signals. *The International Journal of Advanced Manufacturing Technology*, **28**(9-10): 855–862.

ZIO E. 2021. Prognostics and Health Management (PHM): where are we and where do we (need to) go in theory and practice. *Reliability Engineering & System Safety*, p. 108119.

How to cite

ASSAF R, DO P & SCARF P. 2022. A Diagnostics and Prognostics framework for Multi-Component Systems with Wear Interactions: Application to a Gearbox-platform. *Pesquisa Operacional*, **42** (nspe1): e264770. doi: 10.1590/0101-7438.2022.042nspe1.00264770.